CERN-ACC-NOTE-2020-0046
rongrong.cai@cern.ch

Simulations of particle loss due to hollow e-lens and non-linearities for the HL-LHC

R. Cai[1], *D. Mirarchi*[2], *C. Tambasco*[3], *T. Pieloni*[4],
CERN, Geneva, Switzerland
[1] *also at Imperial College London, London, UK*
[2] *also at The University of Manchester, Manchester, UK*
[3] *and* [4] *also at EPFL, Lausanne, Switzerland*

Abstract

Simulations on the effects of an electron lens (e-lens) on the halo population depletion have been carried out for the High Luminosity LHC (HL-LHC). In particular, the different operational modes, and the interaction with the non-linearities introduced by octupoles and chromaticity have been explored.

This study has found that the random activation of the electron beam removes completely the halo above its inner radius on a timescale of 10 s. For all other operational modes, the octupole current variation increases the loss to higher values and to different rates depending on the specific mode and current value. Also, the increase of chromaticity causes a growth in population loss. Finally, an estimation is given for chromaticity and octupole current at HL-LHC baseline values.

Geneva, Switzerland
September 25, 2020

Contents

1 Introduction

In the CERN Large Hadron Collider (LHC), there exists a system of collimators used to dispose of halo particles in a controlled and safe manner. It plays an essential role in the protection of the machine. The different elements of the system are supposed to intercept the particles preventing them from being lost in the cold aperture. However, a complete absorption of all particles interacting with a collimator is not possible. The "leakage" from the collimators to the machine aperture can be quantified with the so-called cleaning inefficiency, defined as the probability for a particle interacting with a collimator of being lost on the superconducting magnets [1]. The current LHC collimation system [2] has a cleaning inefficiency on the order of 10^{-4} and the energy stored in the beams reaches beyond 300MJ [3]. In the High Luminosity LHC (HL-LHC), the stored beam energy will reach around 700 MJ [4]. Special attention has been paid to the energy stored in the tails of the beam. Recent studies [5] at the LHC have shown that the particle distribution would be better described with a double-Gaussian function than a single-Gaussian one. This means that the energy stored in the tails will be larger than expected if the HL-LHC beams also follow the same double-Gaussian distribution as seen for the LHC measurements. In particular, the energy for beams

in the HL-LHC configuration would have a stored energy of around 30 MJ above $\approx 3.5\,\sigma$ [6]. This level of stored beam energy increases the dangers of potential damage from the beam tails. The potential risks include loss spikes and beam dumps caused by orbit jitters and crab cavity phase slip, potential magnet quench, and permanent damage to collimators [6] [7].

Faced with the challenges presented by the upgrade to HL-LHC, the addition of a hollow electron lens (e-lens) [6] in the collimation hierarchy may improve the current performance. Among the potential benefits, it would allow to mitigate loss spikes, reduce the risks of magnet quench, and also mitigate the effect of crab cavity failures [8]. Additionally, an e-lens will have the advantage of an active control of the beam halo and its impact parameter on collimator jaws. Different setups of the e-lens will allow an active control, for example, concerning the depletion rate which may improve the cleaning performance [6].

The e-lens will be placed as an additional element in the collimation hierarchy. The lens surrounds the beam and its inner radius is set to be smaller than the aperture of the primary collimators. A schematic representation is given in Fig. 1 a. This will allow controlling the depletion of the particles that have an amplitude larger than the inner radius of the lens [6], since ideally there is no electromagnetic field within the inner radius of the lens. In fact, in present conditions, the diffusion rate grows as a function of particle amplitude due to the machine non-linearities [9], although the electromagnetic interactions of the beam particles with the electron lens provide additional kicks that would enhance the diffusion rate. As a consequence, the beam population in the tails and the loss spikes will decrease. These two effects are illustrated in Fig. 1 b.

Since the region of operation of the e-lens mainly covers the part where the non-linearities of the machine are the greatest, this study proposes to investigate the interaction between the non-linearities in the optics and the e-lens. In particular, on a timescale of 10 s, the population depletion and the particle distribution evolution are studied. The non-linearities involved are those caused by different octupole currents and chromaticity values. However, beam-beam effects are not included in this study.

In practice, it is also possible to tune the activation of the e-lens at different turns to create different pulsing patterns. Each pulsing pattern would constitute an operational mode. The electron beam current would only change on a turn-to-turn basis according to the pulsing pattern. The various operational modes have also been included, since it has been confirmed by previous studies (e.g. [10] and [11]) that there is a difference in the performance for the different operational modes.

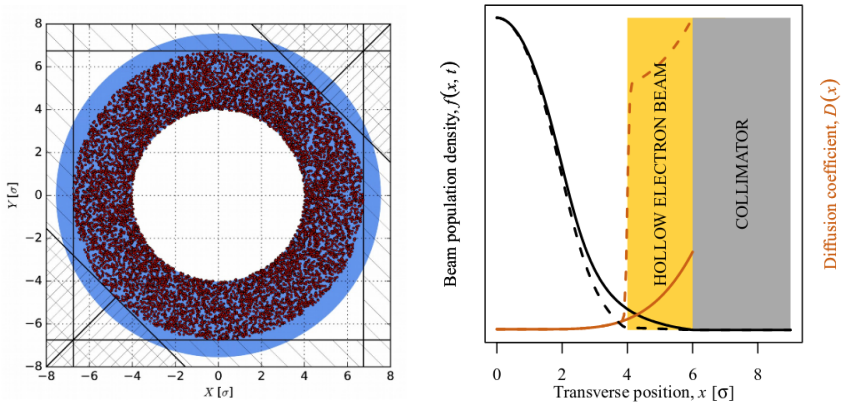

(a) (b)

Fig. 1: Schematic representation of the transverse section of an e-lens (a). The red dots represent the tail particles, the solid lines the different types of collimator and the shaded blue area the electron beam. The beam population without e-lens (solid black line) and with e-lens (dashed black line) and the diffusion rate without e-lens (solid brown line) and with e-lens (dashed brown line) are plotted qualitatively against the particle amplitude in (b).

2 Method and simulation setup

2.1 Optical parameters

These simulations have been carried out by using MAD-X [12] and SixTrack [13], where MAD-X generates input files regarding the optics used by SixTrack to perform particle tracking. For this study the optics of the HL-LHC version 1.3 [14] has been used. In particular, the optics scheme used is the `opt_150_150_-150_150_thin.madx`, referring to the baseline collision optics. One single beam has been simulated to go through the hollow electron lens. The beam travels at the top energy of 7 TeV and the beam-beam interaction has not been included, in order to study what happens before collision and to separate the various influencing factors to obtain a more thorough understanding. The optics has been chosen to be as complete as possible and field errors have also been included to the following elements: MBRB, MBRC, MBRS, MBX, MBW, MQW, MQTL, MQMC, MQX, MQY, MQM, MQML, MQ, MQXF, MCBXF and MBRD. However, in generating the input optics with MAD-X for SixTrack only one seed (seed 1) has been used. Thus, the following results are subject to the particular error fields generated with that seed. Concerning the collimation system, only two primary collimators are positioned at a distance of 6.7 σ (the emittance used is the nominal HL-LHC emittance of 2.5 μm) one in the vertical and one in the horizontal plane,

since the aim is to merely track losses. These collimators are TCP.D6L7.B1 and TCP.C6L7.B1.

2.2 Electron lens parameters

The hollow electron lens is positioned at a distance of 3292.28 m from IP3, i.e. in IR4. Input value of the inner radius for SixTrack is 0.77 mm, while the outer radius is 1.54 mm. In terms of beam size, the inner radius corresponds approximately to 3 σ. In the implementation of the e-lens element in SixTrack no imperfection, such as residual fields in the hollow region of the electron beam, has been included. The modes studied do not include offsets for the e-lens, i.e. the centre of the lens is perfectly aligned with the centre of the proton beam. Other parameters can be found in Table 1.

Table 1: This table shows some of the relevant parameters of the electron lens.

Current	5 A
Length	3 m
Electron energy	10 keV
Electron distribution	uniform within the ring

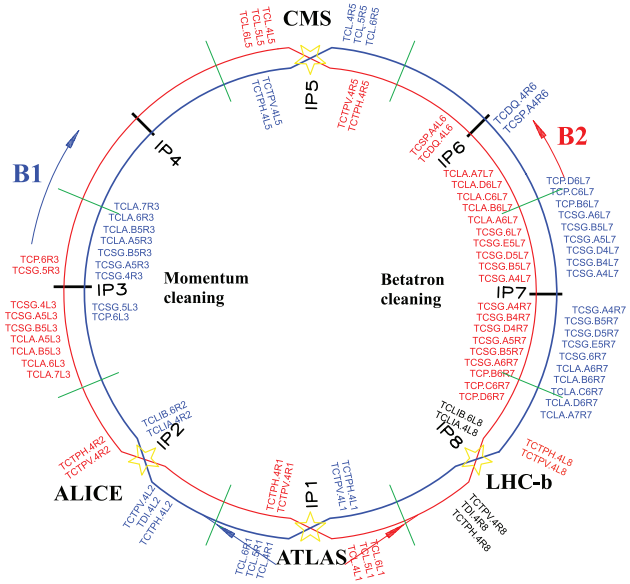

Fig. 2: Layout of the LHC collimation system as of Run 2.

2.3 Initial proton distribution and simulation specifications

Previous measurements at the LHC have revealed that the single-Gaussian can be insufficient to describe the tails of the beam [5]. Instead, a double-Gaussian function has been deemed to be more appropriate. Therefore, the distribution of the particles used is that of a double-Gaussian and the beam ranges up to approximately 10 σ on both sides and in both planes. The double-Gaussian distribution has also been applied to the phase space coordinates. This is done for the beam size at IP3, where the particles start. The initial distribution in the x and y plane is shown in Fig. 3. The percentage of the particles beyond 3 σ occupy approximately 27% of the entire population.

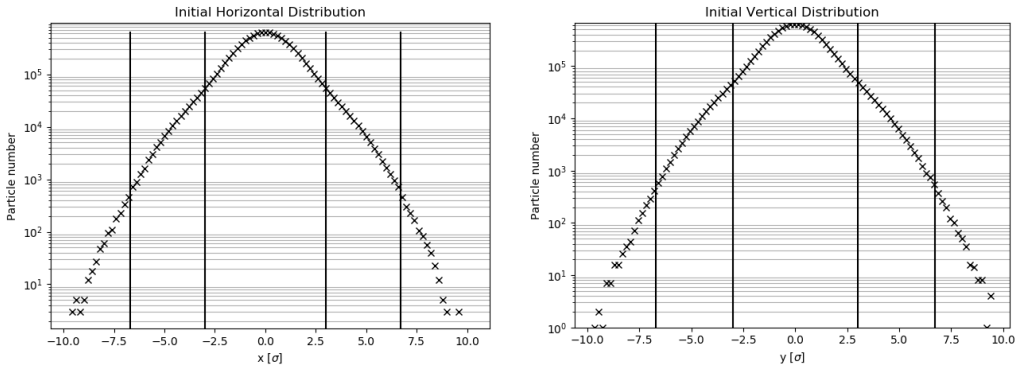

(a) (b)

Fig. 3: Initial particle distribution in both planes (horizontal (a), vertical (b)) plotted in terms of particle number against the particle amplitude expressed in beam size. The vertical bars are positioned at -6.7, -3, 3 and 6.7 σ, respectively for both plots. The 3 σ-distance corresponds to the inner radius of the e-lens and the 6.7 σ-distance corresponds to the positions of the collimators.

For this series of simulations, the proton beam performs a total of 112360 turns ($\sim$ 10 s as one turn takes 89 μs) with 60000 particles tracked. The simulations have been divided into groups of 600 particles each, with 100 sub-simulations. For each simulation the number of surviving particles is recorded turn by turn at IP3, while the information on their distribution is recorded every 11236 turns ($\sim$ 1 s) just before TCP.D6L7.B1. In the population survival studies, the number of lost particles in each sub-simulation has been averaged over the 100 sub-simulations. The distribution information is retrieved by binning the coordinates of the remaining particles every second and fitting the initial double-Gaussian distribution in Eq. (1) to obtain the σ of the distributions.

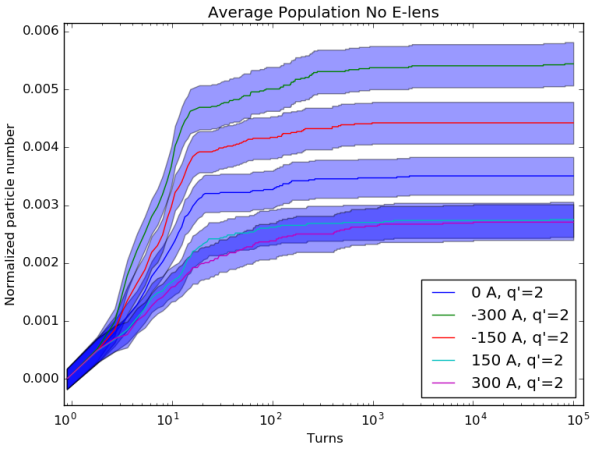

Fig. 4: The fraction of particles lost with respect to the initial number of particles without activating e-lens is plotted in terms of number of turns. The legend shows the particle loss for different the octupole current and chromaticity value, q'. The shaded part of each line corresponds to the uncertainty range.

$$A(0.65e^{-\frac{1}{2\sigma\sqrt{2\pi}}(\frac{x-\mu}{\sigma})^2} + 0.35e^{-\frac{1}{4\sigma\sqrt{2\pi}}(\frac{x-\mu}{2\sigma})^2}) \tag{1}$$

where A is a scaling factor, x is the position of the particle, μ is the expected value and σ is the standard deviation.

3 Simulations without electron lens

In order to explore the dependence of the e-lens performance as a function of octupole current, the tail population depletion without e-lens has been checked. The current of the octupoles was varied from -300 A to 300 A in steps of 150 A. The chromaticity value here was always set to 2.

From the octupole scan, there is a clear natural beam loss. The fraction of particles lost can be found in Fig. 4. In particular the fraction of particles lost at 10 s can be found in Table 2.

With the double-Gaussian fitting, it has been found that there is a change in the shape of the distribution after the first second and then the distribution stays constant with minor fluctuations. The initial scraping is due to the fact that the initial distribution goes beyond 6.7 σ, where the TCPs are placed and to the non-linearities present in the simulated machine. The horizontal distribution of when there is zero octupole current and 2 units of chromaticity is shown in Fig. 5. The apparent loss from the core can be understood by considering the small inner

Current	Percentage of particles lost
-300 A	$(0.54 \pm 0.04)\%$
-150 A	$(0.44 \pm 0.04)\%$
0 A	$(0.35 \pm 0.03)\%$
150 A	$(0.28 \pm 0.03)\%$
300 A	$(0.27 \pm 0.03)\%$

Table 2: This table gives the percentage of particles lost at 10 s when different octupole currents are present and without the e-lens active.

radius of the e-lens and that particles closer to the centre in one plane may be far in the other plane. This consideration also applies to other distribution plots.

As the distribution only stabilised at 1 s after all collimation losses took place, the computed σ of the distribution at later times have been normalised to this value to understand the action of octupoles and chromaticity. The evolution of σ of different configurations with time can be found in Fig. 6. It is clear that the value stays constant for all configurations with a fluctuation of 2%, as expected.

Concerning the scan for different chromaticity values when the e-lens is switched off, the present study has not obtained distinguishable particle loss results after including uncertainties. For all modes, the particle loss reaches a value of approximately $(0.36 \pm 0.03)\%$.

4 Scan of the activation pattern

The e-lens can be turned on at different turns, i.e. the kicks due to the EM field can be applied only at certain turns. The various operational modes apply different activation patterns. This group of simulations is aimed at understanding how these operational modes affect the performance of population depletion. To do so, the octupole current is turned down to zero and chromaticity to 2.

The modes of activation studied here can be divided into four types, as listed below:

- Continuous (DC), during which the device is continuously turned-on and supplying electrons at a constant rate;
- Random (RND), when the device is turned on and off at random turns;
- Pulsed 1 (1t), this mode turns on the device every other turn;
- Pulsed 2 (2t), this mode allows the electrons to be injected every third turn;
- Pulsed 3 (3t), this mode allows the electrons to be injected every fourth turn.

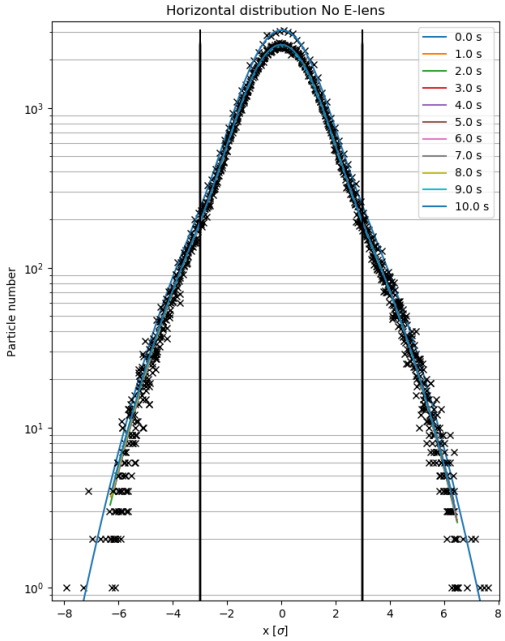

Fig. 5: The horizontal distribution of particle position is shown with the number of particles plotted against the amplitude expressed in beam size. Here, the octupole current is zero and the chromaticity value is 2. The legend shows the time interval. The vertical bars represent the inner radius of the electron beam.

From Fig. 7 we can see a clear hierarchy in the effectiveness of the modes, where the random mode (RND) appears to be the most effective with 26.7 % of loss corresponding to the entire tail population. The full list of hierarchy and the numerical values of particle loss for each mode can be found in Table 3.

The distribution evolution for all modes, except RND, does not have major variation throughout time and it stabilises after the first second at the same value as for the cases when e-lens is deactivated. This behaviour is expected as imperfections in the e-lens are not included and the simulation tools used for these studies only act on the tails. The distribution in the RND mode however, changes due to the strong loss of particles, thus changing the distribution. The horizontal distribution can be found in Fig. 8 for the RND mode and DC mode (as it is representative for other modes too). It is also clear that for the random mode, the e-lens gives a sharp cut at its edges.

The fitted distribution beam size, σ, gives a more concise overview on the evolution of the distribution, namely that for all modes, except the random mode, σ stays constant with a 2 % fluctuation, while the random mode receives a small decrease for both planes. This is shown in Fig. 9.

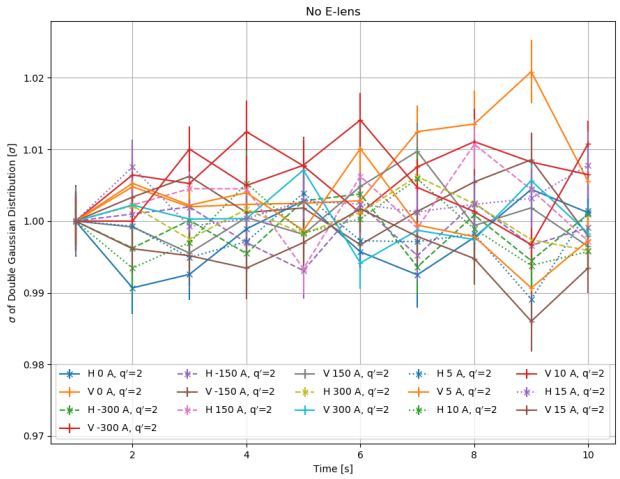

Fig. 6: The fitted value of the distribution σ is plotted against time for different configurations of octupole currents and chromaticities, when the e-lens has been turned off. The error bars represent the standard error of the fit. The legend shows the plane of the distribution ('H' for horizontal plane and 'V' for vertical plane), the octupole current and the value of chromaticity, q'.

5 Octupole current scan

In the octupole scan, different values of octupole magnet strengths have been applied to each of the modes while keeping the chromaticity value at 2 units.

The performance of the random mode is not affected by the change of octupole current with no significant variation during the 10 s of run with respect to the total loss and a loss of approximately 27 % at the end of 10 s. Other modes see a change in the hierarchy of the efficiency in the sense of percentage of particles removed from the tails as a function of octupole current with respect to the one found without e-lens. At small timescales the hierarchy follows the same as that

Mode	Percentage of particle loss	Percentage of tail particle loss
RND	$(26.6 \pm 0.3)\%$	98.5%
DC	$(1.69 \pm 0.07)\%$	6.2%
2t	$(1.30 \pm 0.06)\%$	4.8%
3t	$(1.30 \pm 0.06)\%$	4.8%
1t	$(1.17 \pm 0.05)\%$	4.3%

Table 3: This table gives the percentage of particles lost at 10 s and the percentage of the particles lost with respect to the particles in the tails only when the e-lens is turned on with different modes. There is zero octupole and 2 units of chromaticity.

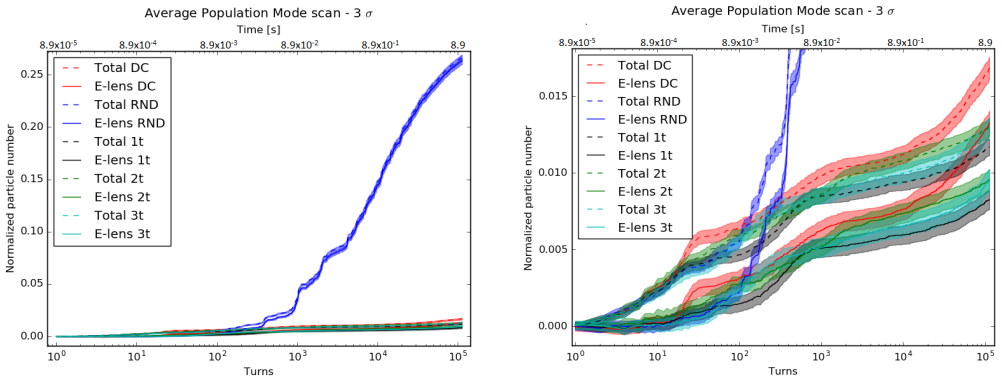

(a) (b)

Fig. 7: The fraction of particles lost with respect to the initial number of particles of the entire population with different modes of e-lens is plotted in terms of number of turns and time. The dashed line represents the total loss, while the continuous line is the loss after the subtraction of the loss when no e-lens has been applied. The legend shows the name of the mode. The shaded part of each line corresponds to the uncertainty range. Fig. (a) shows all modes, while (b) is a zoomed version of (a).

shown by the scenarios with no e-lens. For longer times, the particle loss of some octupole values grows faster and crosses the ones that were originally higher in the ranking. This increase in the speed of tail depletion occurs for different octupole values at different times. Depending on the octupole values and the mode, the loss is also enhanced to a different degree.

From a numerical point of view, the particle loss of all modes, except 3t, does not differ significantly from that of when the octupole current is zero. The detailed results of the remaining population at 10 s can be found in Fig. 10 a. From this plot we can conclude that at least on the 10 s timescale the modes DC, 1t, and 2t keep a constant loss percentage between 0.5 % and 2 %. The final percentage of particles remaining ranges from 2 to 5.5 times the value obtained when there was no e-lens. The random mode maintains a constant performance within the uncertainties.

The case that clearly shows dependency from octupole current variation is 3t, where the positive currents increased the total loss to (4.7 $\pm$ 0.1) % for 150 A and (2.48 $\pm$ 0.08) % for 300 A. The evolution with time is given in Fig. 10 b. For a current of 150 A there is a sharp increase at around 0.01 s. However, this increase, although small, can also be noticed for current 300 A at the timescale of 1 s and for current -300 A at approximately 0.1 s. According to the results obtained with the settings described previously, these changes differ in timescale

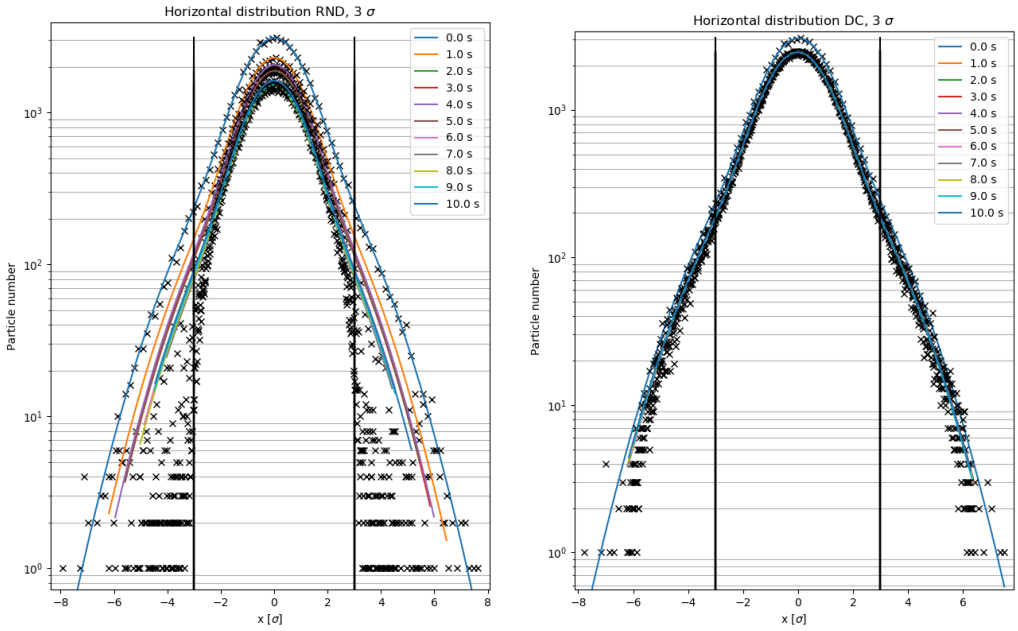

(a) (b)

Fig. 8: The horizontal distribution for RND mode (a) and DC mode (b) is shown. The number of particles is plotted against the amplitude in units of beam size. The legend shows the number of turns, which correspond to approximately 0 s, 1 s, 2 s, etc.

and magnitude. The fact that the current values mostly affected are the positive currents leads to the hypothesis that the configurations with a larger tune spread are the most susceptible to enhancements in population loss.

Regardless of the physical causes, we can conclude that the change in octupole current affects the loss speed in magnitude and the timescales at which this occurs depending on the different mode.

In terms of the particle distribution, there is no significant difference from the zero octupole current case.

6 Chromaticity scan

In the chromaticity scan, the value of octupole current is fixed and the chromaticity value is made to vary from 5 to 15 with steps of 5 units.

For all activation modes (except the random mode) there is a clear increase in the population loss as a function of chromaticity. The case of 3t is illustrated in Fig. 11 a as an example. However, the exact amount of increase is different for

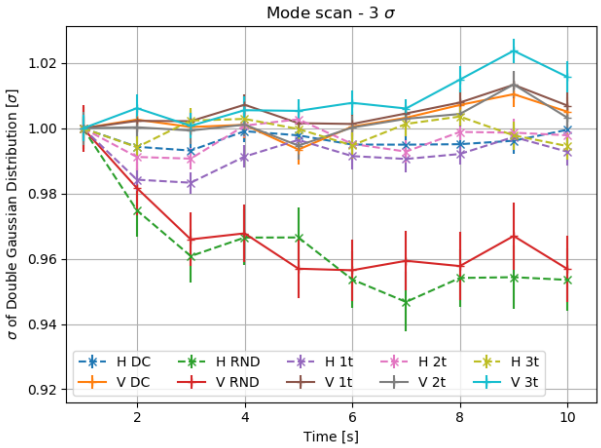

Fig. 9: The σ of the fitted distribution normalized to the value at the first second is plotted against time. The error bars represent the standard error of the fit. The legend gives information on the relevant plane ('H' for horizontal plane and 'V' for vertical plane) and the mode used.

each mode. The random mode remains unaffected. The total loss for the individual modes is indicative of the quantitative differences between the susceptibility of each mode. This is shown in Fig. 11 b. The mode 3t is the most susceptible to chromaticity change. This behaviour can be understood by looking at the fractional part of the tune which is 0.31 and 0.32. Unlike in the octupole scan, all changes in population loss occur at the same timescale of 0.1 s.

The particle distribution evolution is not affected by the variation of chromaticity.

7 Estimations with HL-LHC baseline values

An estimation of the population loss has been made for the octupole current value and the chromaticity value of the baseline design in HL-LHC [15], i.e. $I_{octupole} = -300$ A and chromaticity has a value of 15.

The strong octupole and chromaticity values have caused a change in the hierarchy of efficiency in the activation modes, despite the random mode still being the most efficient one. The evolution of the population loss with time can be found in Fig. 12.

The percentage of population loss in the tails is shown in Table 4.

In terms of particle distribution evolution, no significant change has been observed from the mode scan cases.

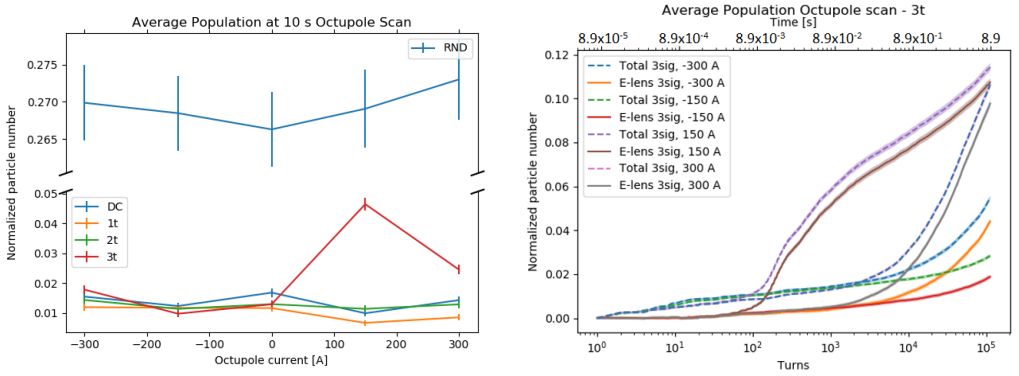

(a) (b)

Fig. 10: In (a) the normalized particle number (fraction of particles lost with respect to the entire population) at 10 s is plotted against the octupole current for different activation modes (in the legend). In (b) the number of particles remaining at each turn normalized to the initial particle number is plotted against the number of turns and the corresponding time for mode 3t. The dashed lines represent the total loss, while the continuous ones represent the loss after the subtraction of the loss when no e-lens has been applied. The legend shows whether it is the total or partial loss (e-lens), the position of the inner radius (3sig, i.e. 3 σ) and the octupole current.

8 Conclusion

This study investigates the dependence of the collimation electron lens (e-lens) performance with respect to the non-linearities introduced by the octupole magnets and high chromaticity operation in a realistic optical setup of the High Luminosity LHC. In particular, the particle loss as a function of turns and the particle distribution per second were explored. No beam-beam effects were included. The configuration included multipole errors, although with only one seed. Only two collimators have been placed horizontally and vertically at the distance of 6.7 σ to track the particle loss. The inner radius of an ideal e-lens was placed at a distance of 3 σ with 5 A of current and an energy of 10 keV. Since previous measurements at the LHC have revealed a particle distribution that would be better described with a double-Gaussian function [5], this distribution is used to generate the initial distribution of the particles. 60000 particles (core and tails) were tracked for 112360 turns (10 s). Different operational modes for the electron lens powering have been explored: continuous (DC), activation at random turns (RND), activation every second turn (1t), activation every third turn (2t) and activation every fourth turn (3t).

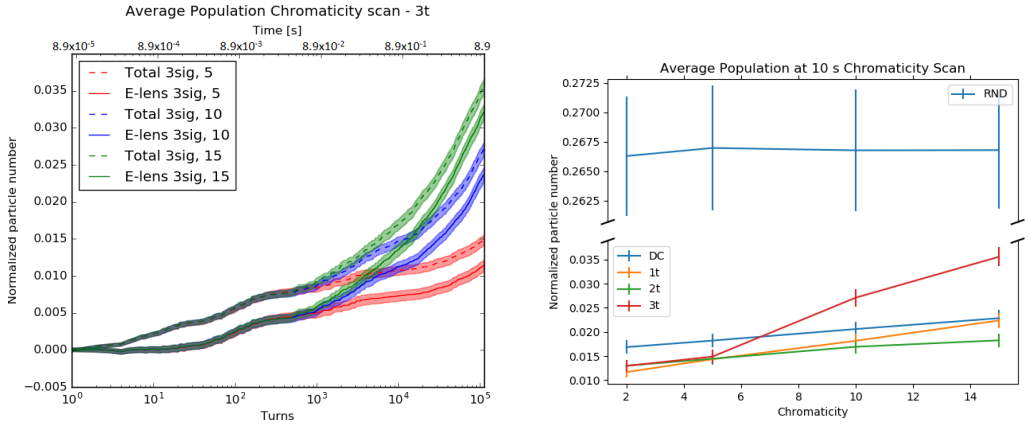

(a) (b)

Fig. 11: In (a) the fraction of particles lost with respect to the initial number of particles of the entire population with different values of chromaticity (in the legend) is plotted in terms of number of turns and time for mode 3t. The shaded part of each line corresponds to the uncertainty range. The dashed line represents the total loss, whereas the continuous line represents the loss after subtracting the loss found in the corresponding no e-lens case. Fig. (b) plots the fraction of particles lost at 10 s against the chromaticity value for different modes.

When no e-lens is present the particle loss is most pronounced for large and negative octupole currents (approximately 0.54 % of the total number of particles lost at 10 s when $I_{octupole} = -300$ A) and least pronounced for large and positive octupole currents (around 0.27 % of the total number of particles lost at 10 s when $I_{octupole} = 300$ A). The particle distribution would stabilise after 1 s (no data is recorded for time interval shorter than 1 s) with a fluctuation of 2 % of the stable beam size.

When there is zero octupole current and 2 units of chromaticity, most operational modes have a particle loss between 1 and 2 % with respect to the initial particle number, except for the RND. The random mode has a loss of around 27 %, which corresponds exactly to the percentage of particles lying beyond 3 σ in the initial distribution. The performance of RND is not affected by the variation of octupole current nor chromaticity. The distribution evolution for other modes does not change significantly from when there is no e-lens. This situation repeats for octupole and chromaticity scans as well.

The variation of octupole current changes the hierarchy of performance of the operational modes. It gives rise to an increase in population loss which occurs at different timescales, with a different magnitude and rate for different octupole currents and operational modes. A possible explanation may be found in the global

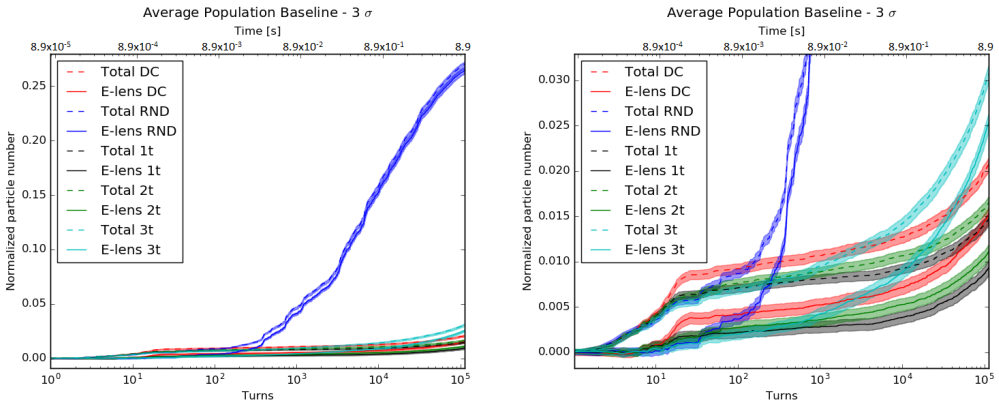

(a) (b)

Fig. 12: The fraction of particle lost with respect to the initial number of particles of the entire population with different modes for the baseline configuration is plotted in terms of number of turns and time. The dashed line represents the total loss, while the continuous line is the loss after the subtraction of the loss when no e-lens has been applied. The legend shows name of the mode. The shaded part of each line corresponds to the uncertainty range. Fig. (a) shows all modes, while (b) is a zoomed version of (a).

tune spread. The most susceptible mode is 3t which sees a growth of loss from approximately 2 % of the initial population at zero current to almost 5 % at a current of -150 A. Other modes maintain a loss range between 0.5 % and 2 % at 10 s.

When there is a variation of the chromaticity, the positive dependence of the loss with respect to the chromaticity values is clear. All modes (except RND) show different degrees of increase in loss with the growth of chromaticity values. The 3t mode remains the most susceptible, reaching approximately 3.5 % of loss with respect to the initial population with $q' = 15$ at 10 s.

Finally, by setting the octupole current to -300 A and chromaticity to 15, the population loss increases up to between 1.47 and 3.07 % of initial population at 10 s.

9 Outlook

The present study is limited by the lack of statistics in the implementation of multipole errors. Hence, more seeds should be used in the future to check whether the results presented here have been significantly affected by this particular setup. The results can be further improved by also increasing the total number of particles tracked.

Mode	Percentage of particle loss	Percentage of tail particle loss
RND	$(27.0 \pm 0.3)\%$	100%
3t	$(3.07 \pm 0.09)\%$	11.4%
DC	$(2.07 \pm 0.07)\%$	7.7%
2t	$(1.65 \pm 0.07)\%$	6.1%
1t	$(1.47 \pm 0.07)\%$	5.4%

Table 4: This table gives the total percentage of the particles lost at 10 s in terms of the initial number of particles and the percentage of the particles lost with respect to the particles in the tails only. These values are given for every activation mode.

The octupole scan results show the importance of timescales and how the efficiency may vary depending on this. Therefore, longer timescales should be investigated to check the variation of time dependence of the various modes and machine non-linearities.

Dependence on other e-lens parameters, e.g. higher pulsing intervals, e-lens strength modulation with betatron frequency or otherwise, electron current, e-lens radius etc may be explored. Future studies may also try to recreate scenarios closer to operational ones.

References

[1] Roderik Bruce, Marco D'Andrea, Nuria Martinez, Arkadiusz Gorzawski, Alessio Mereghetti, Daniele Mirarchi, Marcin Patecki, Roberto Rossi, Belen Salvachua, Matteo Camillocci, Joschka Wagner, Hector Morales, Gabriella Azzopardi, and Gianluca Valentino. Beam losses, lifetime and collimator hierarchy. In *Proc. of the 8th Evian Workshop*, number CERN-ACC-2019-012, Evian, France, 12 – 14 December 2017. `https://www.um.edu.mt/library/oar/handle/123456789/58906`.

[2] R W Assmann, O Aberle, G Bellodi, A Bertarelli, C Bracco, H Braun, M Brugger, S Calatroni, R Chamizo, Alessandro Dallocchio, B Dehning, A Ferrari, P Gander, A Grudiev, E B Holzer, J B Jeanneret, J M Jiménez, M Jonker, Y Kadi, K Kershaw0, J Lendaro, Jacques Lettry, R Losito, M Magistris, A Masi, M Mayer, E Métral, R Perret, C Rathjen, S Redaelli, G Robert-Démolaize, S Roesler, F Ruggiero, M Santana, P Sievers, M Sobczak, A Tsoulou, V Vlachoudis, T Weiler, I S Baishev, and I Kurochkin. The final collimation system for the LHC. (LHC-PROJECT-Report-919. CERN-LHC-Project-Report-919):4 p, Jul 2006. `http://cds.cern.ch/record/972336`.

[3] N. Fuster Martinez, A. Abramov, G. Azzopardi, A. Gorzawski, E. Belli, C. Boscolo-Meneguolo, R. Bruce, M. D'Andrea, M. Di Castro, M. Fiascaris, A. Fomin, P. D. Hermes, H. Garcia-Morales, R. Kwee-Hinzmann, D. Kodjaandreev, A. Mereghetti, D. Mirarchi, J. Molson, L. Nevay, E. Quaranta, M. Patecki, S. Redaelli, A. Rossi, R. Rossi, B. Salvachua, M. Solfaroli Camillocci, G. Valentino, A. Valloni, and J. Wagner. Run 2 collimation overview. In *Proc. of the 9th Evian Workshop*, Evian, France, 30 January – 1 February 2019. https://indico.cern.ch/event/751857.

[4] G Apollinari, I Béjar Alonso, O Brüning, M Lamont, and L Rossi. *High-Luminosity Large Hadron Collider (HL-LHC): Preliminary Design Report*. CERN Yellow Reports: Monographs. CERN, Geneva, Switzerland, 2015. https://cds.cern.ch/record/2116337.

[5] P Racano. Review of halo measurements at large hadron collider with collimator scans. In *8th HL-LHC Collaboration Meeting*, Geneva, Switzerland, 15 – 18 October 2018. https://indico.cern.ch/event/742082/contributions/3142444/.

[6] D Mirarchi, H Garcia Morales, A Mereghetti, S Redaelli, Joschka Wagner, W Fischer, X Gu, and G Stancari. Hollow electron-lens assisted collimation and plans for the LHC. (FERMILAB-CONF-18-311-AD-APC):TUP1WE02. 7 p, 2018. https://cds.cern.ch/record/2640825.

[7] S Redaelli. Introduction to the review for needs of a hollow e-lens for the HL-LHC. In *Review of the needs for a hollow e-lens for the HL-LHC*, Geneva, Switzerland, 6 – 7 October 2016. https://indico.cern.ch/event/567839/contributions/2295242/attachments/1349314/2036639/SRedaelli_2016-10-06_print.pdf.

[8] D Wollmann. Potential failure scenarios that can lead to very fast orbit changes and machine protection requirements for hl-lhc operation. Review of the needs for a hollow e-lens for the HL-LHC, Geneva, Switzerland, 6 – 7 October 2016. https://indico.cern.ch/event/567839/contributions/2295329/attachments/1349889/2037271/20161006_HollowELReview_MP_FastFailures_V2.pdf.

[9] Giulio Stancari. New methods of particle collimation in colliders. In *Proceedings of the 2011 Meeting of the Division of Particles and Fields of the American Physical Society (APS/DPF 2011)*, number FERMILAB-CONF-11-506-AD-APC, page 9 p, Providence, Rhode Island, USA, 9 – 13 August 2011. https://arxiv.org/abs/1110.0144.

[10] V Previtali, G Stancari, A Valishev, and S Redaelli. Numerical simulations of a hollow electron lens as a scraping device for the LHC.

(FERMILAB-CONF-13-154-APC):MOPWO044. 3 p, May 2013. https://cds.cern.ch/record/2010130.

[11] M Fitterer, G Stancari, A Valishev, R Bruce, S Papadopoulou, G Papotti, D Pellegrini, S Redaelli, D Valuch, and J F Wagner. Hollow Electron Beam Collimation For HL-LHC - Effect On The Beam Core. (FERMILAB-CONF-16-387-AD. NAPAC-2016-WEA1CO04):WEA1CO04. 4 p, 2017. https://cds.cern.ch/record/2314321.

[12] Mad - methodical accelerator design. https://mad.web.cern.ch/mad/, 2019.

[13] Sixtrack – 6d tracking code. http://sixtrack.web.cern.ch/SixTrack/.

[14] R. De Maria *et al.* HLLHCV1.3 optics repository. http://lhc-optics.web.cern.ch/lhc-optics/HLLHCV1.3/.

[15] Elias Metral, Sergey Antipov, Fanouria Antoniou, Robert Barrie Appleby, Gianluigi Arduini, Javier Barranco Garcia, Philippe Baudrenghien, Nicolo Biancacci, Chiara Bracco, Roderik Bruce, Xavier Buffat, Rama Calaga, Lee Robert Carver, Elena Chapochnikova, Matthew Paul Crouch, Riccardo De Maria, Stephane Fartoukh, Davide Gamba, Massimo Giovannozzi, Patrik Goncalves Jorge, Wolfgang Hofle, Giovanni Iadarola, Nikos Karastathis, Alexandre Lasheen, Themistoklis Mastoridis, Luis Eduardo Medina Medrano, Alessio Mereghetti, Daniele Mirarchi, Bruno Muratori, Parthena Stefania Papadopoulou, Yannis Papaphilippou, Dario Pellegrini, Tatiana Pieloni, Stefano Redaelli, Giovanni Rumolo, Benoit Salvant, Matteo Solfaroli Camillocci, Claudia Tambasco, Rogelio Tomas Garcia, and Daniel Valuch. Update of the HL-LHC operational scenarios for proton operation. (CERN-ACC-NOTE-2018-0002):42 p, Jan 2018. http://cds.cern.ch/record/2301292.